

⁹J. A. Armstrong *et al.*, Nucl. Phys. **B41**, 445 (1972); H. Meyer *et al.*, Phys. Lett. **33B**, 189 (1970); D. O. Caldwell *et al.*, Phys. Rev. Lett. **23**, 1256 (1969); **24**, 796 (E) (1970); D. O. Caldwell *et al.*, Phys. Rev. D **7**, 1362 (1972); photonuclear data index, NBS Report No. NBS 322, 1970 (unpublished), and references cited therein.

¹⁰It is amusing to notice that this result is again consistent with Harari's argument, in which one can switch

off the strong interactions (leaving behind an elementary neutron and proton), since the deuteron becomes unbound in this limit. In this case, the proton and neutron $\alpha=0$ terms are given by their respective Thomson limits, while that of the deuteron is the sum of the two. This picture becomes suspect when one considers the nucleons to be composite systems.

PHYSICAL REVIEW D

VOLUME 8, NUMBER 1

1 JULY 1973

Differential Cross Sections for Pair Production by Photons on Electrons

S. Jarp* and K. J. Mork

Institute of Physics, University of Trondheim, Norges Laererhøgskole, Trondheim, Norway

(Received 5 February 1973)

The cross section for pair production by unpolarized photons on free, unpolarized electrons is differential in four nontrivial variables. This cross section is integrated numerically over two or three of the variables, and various energy spectra and angular distributions are obtained. The calculations are restricted to low photon energies, below 5 MeV, where effects of recoil and exchange are important and may be observed.

INTRODUCTION

The differential cross section for pair production by unpolarized photons on free, unpolarized electrons has been calculated earlier,¹ and the total cross section has been obtained by Mork.² It has been shown that for high photon energies, above a few hundred MeV, the difference between the cross sections for production of pairs on a heavy target and on a light target vanishes, since almost all pairs are created at low-momentum transfers and the recoil of the target particle is negligible. Also exchange effects are negligible at high energies. According to Ref. 2, exchange effects may also be neglected for lower photon energies (down to about 6 MeV), and the triplet cross section is well represented by the Borsellino formula³ which only includes recoil effects. This has been shown for the total cross section, and it must also be true for the differential cross sections except for some special geometries.

For photon energies below about 6 MeV, both exchange and γ - e diagrams are important, and these effects reduce the triplet cross section considerably compared to the Borsellino cross section. In order to verify these effects, it is therefore of interest to study the triplet cross section for energies between threshold ($4mc^2$) and 6 MeV. This energy region also has the advantage in that screening, binding, and Coulomb corrections should be small.

At present, a group at the University of Cler-

mont is making detailed investigations of the triplet process for low photon energies by using a streamer-chamber technique,⁴ and motivated by this experiment, we have calculated various cross sections differential in one or two variables. As has been shown by the experiment, it is imperative to make use of the kinematical relations for the triplet process in order to separate real triplets from false ones. For some cases the kinematical limits of the triplet variables can be given by simple analytic expressions (cf. Ref. 1). Some other more complicated cases are discussed below.

We use units in which $\hbar=1$, $c=1$, $m=1$.

I. THE DIFFERENTIAL CROSS SECTION

The differential cross section for unpolarized particles is given by

$$d\sigma = \frac{\alpha r_0^2}{|\mathbf{p} \cdot \mathbf{k}|} \frac{d^3p_1 d^3p_2 d^3p_3}{4\pi^2 \epsilon_1 \epsilon_2 \epsilon_3} \delta^4(p+k-p_1-p_2-p_3) X, \quad (1.1)$$

where X is a function of invariant products and it is given in Ref. 1. The four-momenta of the incoming photon and electron are k and p , and the four-momenta of the outgoing electrons and positron are p_1 , p_2 , and p_3 , respectively. Electron energies and momenta are ϵ , ϵ_1 , ϵ_2 and \vec{p} , \vec{p}_1 , \vec{p}_2 ; positron and photon energies and momenta are ϵ_3 , ω and \vec{p}_3 , \vec{k} , respectively.

The cross section given by Eq. (1.1) contains nine independent variables. Four variables are easily integrated when we use the δ function. One variable is a trivial azimuthal angle since we have symmetry around \vec{k} . It is too complicated to do the remaining integrations analytically and we therefore use numerical integration.

Present experiments on triplet production are made in the laboratory system where the initial electron is approximately at rest. We therefore perform the integrations using laboratory variables. The total cross section, however, is most easily obtained in the center-of-mass system as has been shown in Ref. 1. We use the Monte Carlo method of integration.

II. ENERGY DISTRIBUTIONS, $d\sigma/d\epsilon_3$ and $d\sigma/d\epsilon_2$

The triplet cross section is of course symmetric in the variables of the two final electrons, and it is in principle not possible to distinguish the produced electron from the recoiling one. For high photon energies, the pairs are dominantly produced at low-momentum transfers, and it is then meaningful to distinguish the low-energy recoiling electron from the produced high-energy electron. For our low photon energies, the recoiling electron cannot be identified, and we have thus two energy distributions: $d\sigma/d\epsilon_2$, which is the energy spectrum of one of the final electrons, and $d\sigma/d\epsilon_3$, which is the energy spectrum of the positron.

Calculating $d\sigma/d\epsilon_3$, we use as variables of integration the quantities x , y , ϵ_2 , and φ_2 where x and y are the cosines of the angles between \vec{k} and \vec{p}_3 and \vec{p}_2 , respectively, and φ_2 is the azimuthal angle of \vec{p}_2 with \vec{k} as polar axis. The phase space has been obtained by Mork¹ and Jarp,⁵ and we find the cross section

$$\frac{d\sigma}{d\epsilon_3} = \frac{\alpha r_0^2}{2\pi\omega} |\vec{p}_3| \int_{x_-}^1 dx \int_{\epsilon_2^-}^{\epsilon_2^+} |\vec{p}_2| d\epsilon_2 \times \int_{y_-}^{y_+} dy \frac{X}{[a_1(y_+ - y)(y - y_-)]^{1/2}}, \quad (2.1)$$

where the trivial integration over φ_2 has been performed. The limits of y are

$$y_{\pm} = [b_1 \pm (b_1^2 - a_1 c_1)^{1/2}] a_1^{-1}, \quad (2.2)$$

where

$$\begin{aligned} a_1 &= |\vec{p}_2|^2(\omega^2 + |\vec{p}_3|^2 - 2\omega|\vec{p}_3|x), \\ b_1 &= A_1 |\vec{p}_2|(\omega - |\vec{p}_3|x), \\ c_1 &= A_1^2 - |\vec{p}_2|^2 |\vec{p}_3|^2 (1 - x^2), \\ A_1 &= |\vec{p}_3| \omega x - (\omega + m)(\epsilon_2 + \epsilon_3 - m) + \epsilon_2 \epsilon_3. \end{aligned} \quad (2.3)$$

The limits of ϵ_2 are

$$\epsilon_2^{\pm} = [b_2 \pm (b_2^2 - a_2 c_2)^{1/2}] a_2^{-1}, \quad (2.4)$$

where

$$\begin{aligned} a_2 &= 2[|\vec{p}_3| \omega x - (\omega + m)(\epsilon_3 - m)], \\ b_2 &= (\omega + m - \epsilon_3)[|\vec{p}_3| \omega x - (\omega + m)(\epsilon_3 - m)], \\ c_2 &= m^2(\omega^2 + |\vec{p}_3|^2 - 2\omega|\vec{p}_3|x) \\ &\quad + [|\vec{p}_3| \omega x - (\omega + m)(\epsilon_3 - m)]^2. \end{aligned} \quad (2.5)$$

The maximum angle between \vec{k} and \vec{p}_3 for given ϵ_3 is determined by

$$x_- = [(\omega + m)(\epsilon_3 - m) + 2m^2] (|\vec{p}_3| \omega)^{-1}, \quad (2.6)$$

and the positron energy may vary between the limits

$$\epsilon_3^{\pm} = \{\omega^2 - m^2 \pm \omega[\omega(\omega - 4m)]^{1/2}\} (2\omega + m)^{-1}. \quad (2.7)$$

It should be noted that since we now integrate over all final states of the two identical electrons, we count identical final states twice, and we therefore have divided the cross section by a factor of 2.

For the details of the numerical integrations in Eq. (2.1) we refer to Jarp.⁵ We have calculated $d\sigma/d\epsilon_3$ for photon energies $\omega = 4.4, 5.12, 7.0, 10.0 mc^2$. The results are shown in Fig. 1.

The calculation of the electron energy spectrum $d\sigma/d\epsilon_2$ is very similar to the calculation of $d\sigma/d\epsilon_3$. Since the phase space is symmetric in p_2 and p_3 , the cross section $d\sigma/d\epsilon_2$ is given by Eq. (2.1), if we interchange ϵ_2 , $|\vec{p}_2|$, and x by ϵ_3 , $|\vec{p}_3|$, and y , respectively, in this and the following equations. The quantity X is of course left unchanged. We also multiply by a factor of 2, since we now do not integrate over identical final states. The results are shown in Fig. 2, where $d\sigma/d\epsilon_2$ is given for photon energies $\omega = 4.4, 5.12, 7.0, 10.0 mc^2$.

III. ANGULAR DISTRIBUTIONS $d\sigma/dx$ and $d\sigma/dy$

The angular distribution of the positron is $d\sigma/dx$, where $x = \cos\theta_+$, and θ_+ is the angle between \vec{k} and \vec{p}_3 . This cross section is easily obtained from Eq. (2.1), if we interchange the order of integrating x and ϵ_3 in this expression. We find

$$\frac{d\sigma}{dx} = \frac{\alpha r_0^2}{2\pi\omega} \int_{\epsilon_3^-}^{\epsilon_3^+} |\vec{p}_3| d\epsilon_3 \int_{\epsilon_2^-}^{\epsilon_2^+} |\vec{p}_2| d\epsilon_2 \times \int_{y_-}^{y_+} dy \frac{X}{[a_1(y_+ - y)(y - y_-)]^{1/2}}, \quad (3.1)$$

where the limits of ϵ_3 are

$$\epsilon_3^{\pm} = \frac{m[\omega^2 - m^2 \pm \omega x(\omega^2 x^2 - 4\omega m)^{1/2}]}{(\omega + m)^2 - \omega^2 x^2}, \quad (3.2)$$

and x may vary between one and the lower limit

$$x_- = 2(m/\omega)^{1/2}. \quad (3.3)$$

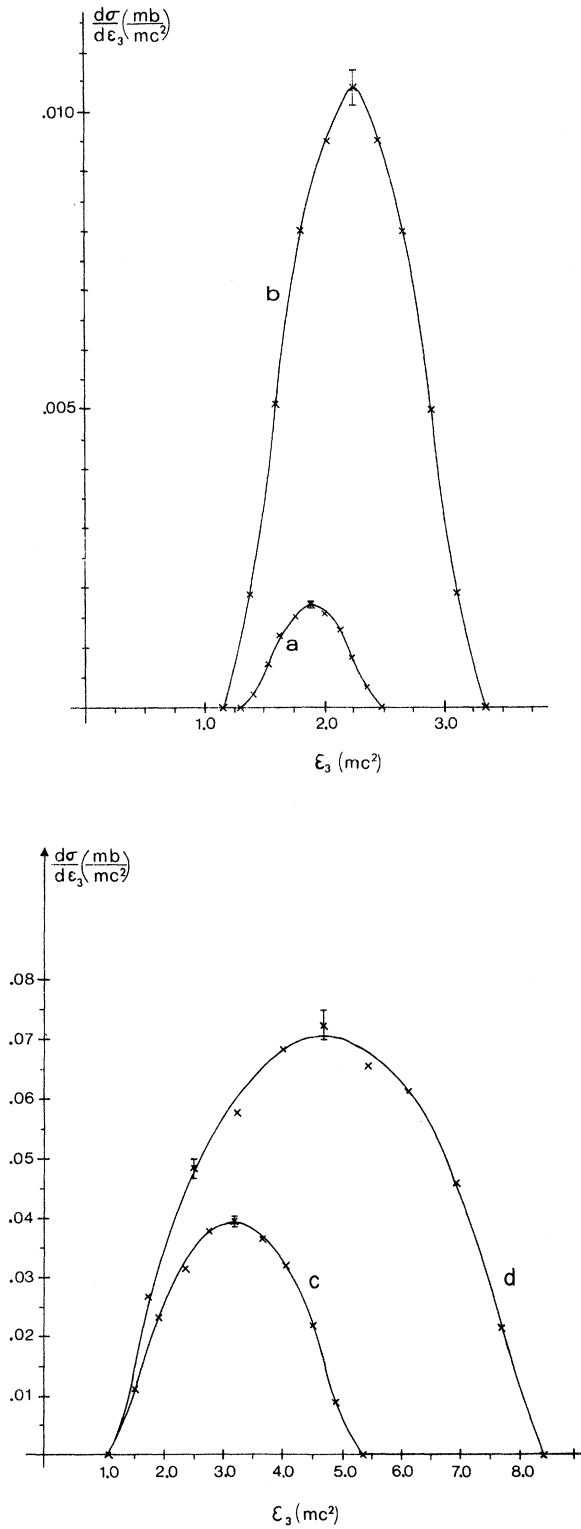


FIG. 1. The positron energy spectrum $d\sigma/d\epsilon_3$ as a function of ϵ_3 in units of mc^2 . The curves a, b, c, and d correspond to lab. photon energies $\omega = 4.4, 5.12, 7.0$, and 10.0mc^2 , respectively.

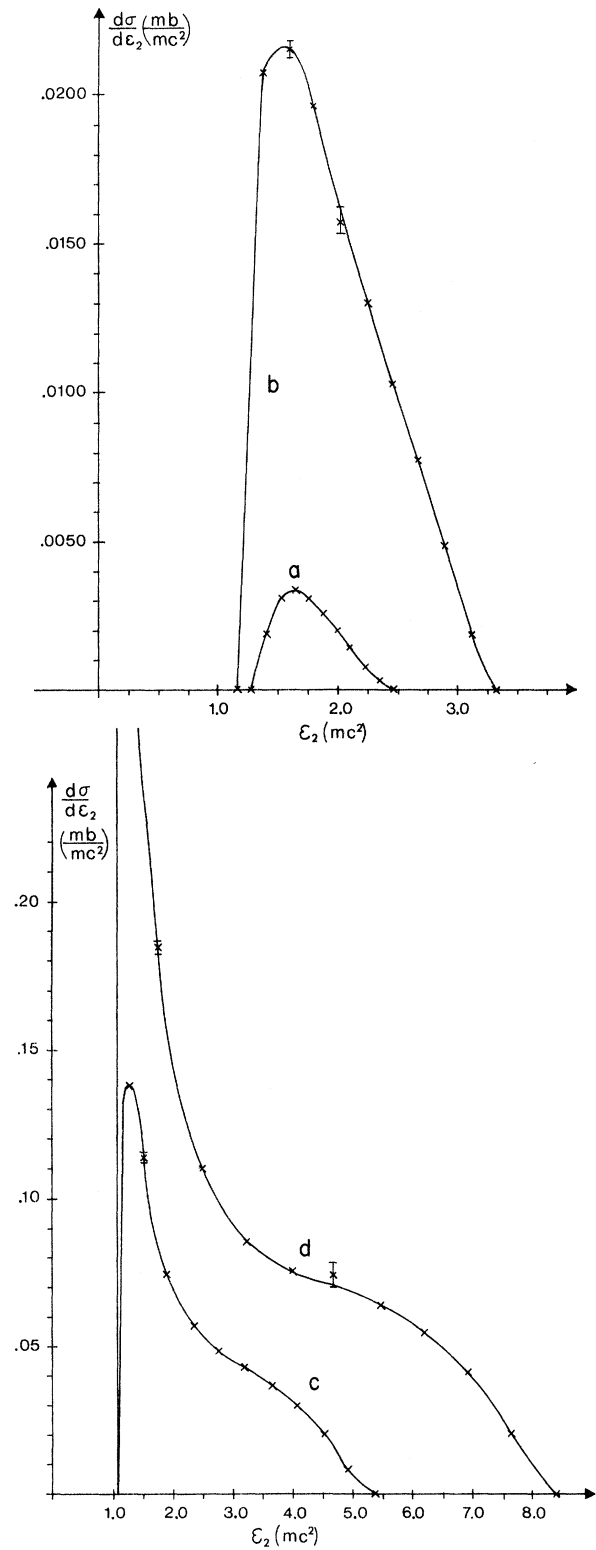


FIG. 2. The electron energy spectrum $d\sigma/d\epsilon_2$ as a function of ϵ_2 in units of mc^2 . The curves a, b, c, and d correspond to lab. photon energies $\omega = 4.4, 5.12, 7.0$, and 10.0mc^2 , respectively.

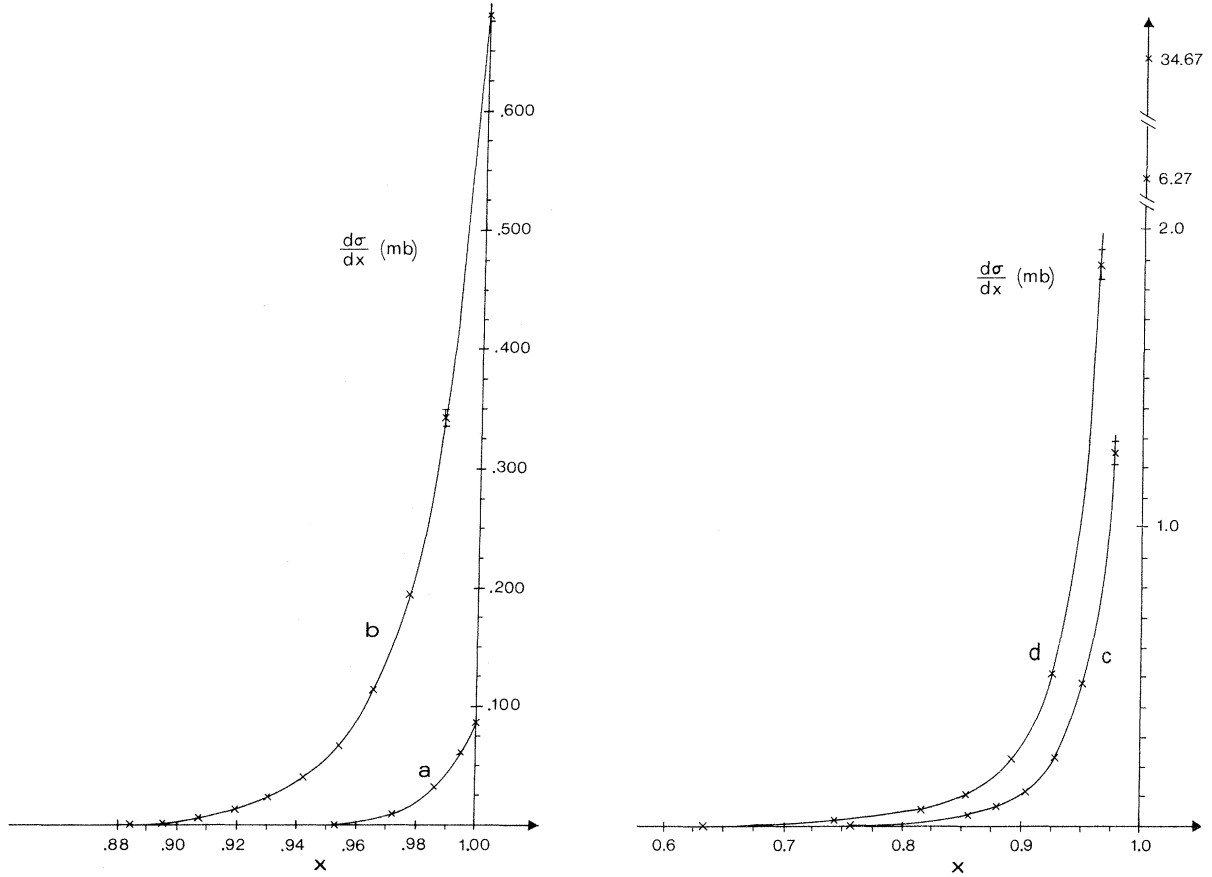


FIG. 3. The positron angular distribution $d\sigma/dx$, where $x = \cos\theta_+$, and θ_+ is the angle between \vec{k} and \vec{p}_3 . The curves a, b, c, and d correspond to photon energies $\omega = 4.4, 5.12, 7.0,$ and $10.0 mc^2$, respectively.

The results are shown in Fig. 3 for photon energies $\omega = 4.4, 5.12, 7.0,$ and $10.0 mc^2$.

The angular distribution of one of the final electrons is $d\sigma/dy_+$, where $y = \cos\theta_-$, and θ_- is the angle between \vec{k} and \vec{p}_2 . We may again use the symmetry in p_2 and p_3 of the phase space (cf. the discussion at the end of Sec. II). The results are shown in Fig. 4.

IV. THE OPENING-ANGLE DISTRIBUTION $d\sigma/dz$

The opening-angle distribution is $d\sigma/dz$, where $z = \cos\theta_{+-}$ and θ_{+-} is the angle between the positron momentum \vec{p}_3 and the momentum \vec{p}_2 of one of the final electrons. To calculate this cross section, it is necessary to integrate over the variables keeping z fixed. The kinematical equations now lead to very complicated relations for the limits of the variables, and we shall discuss this in some detail. The cross section $d\sigma$ is proportional to

$$d^9\rho = \frac{d^3p_1 d^3p_2 d^3p_3}{\epsilon_1 \epsilon_2 \epsilon_3} \delta(p+k-p_1-p_2-p_3). \quad (4.1)$$

Using the δ function to integrate over d^3p_1 , we find

$$d^6\rho = \frac{d^3p_2 d^3p_3}{\epsilon_1 \epsilon_2 \epsilon_3} \delta(\omega+1-\epsilon_1-\epsilon_2-\epsilon_3), \quad (4.2)$$

where

$$\epsilon_1 = [m^2 + (\vec{k} - \vec{p}_2 - \vec{p}_3)^2]^{1/2}. \quad (4.3)$$

Writing

$$d^3p_2 d^3p_3 = |\vec{p}_2| \epsilon_2 d\epsilon_2 |\vec{p}_3| \epsilon_3 d\epsilon_3 dx d\phi_3 dy d\phi_2, \quad (4.4)$$

where the variables are defined in Sec. I (ϕ_3 is the azimuthal angle of \vec{p}_3), we introduce instead of ϕ_3 , the variable $\phi = \phi_3 - \phi_2$ which makes ϕ_2 a trivial variable. Then we introduce instead of ϕ , the variable

$$z = \cos\theta_{+-} = xy + [(1-x^2)(1-y^2)]^{1/2} \cos\phi, \quad (4.5)$$

and after integration over y , using the δ function in Eq. (4.2), we find

$$d^4\rho = 2\pi \frac{|\vec{p}_3| d\epsilon_3 d\epsilon_2 dx dz}{\omega [1-x^2-y^2-z^2+2xyz]^{1/2}} \quad (4.6)$$

where y is determined in terms of ϵ_2 , ϵ_3 , x , and z by Eq. (4.3), and the condition $\omega + 1 - \epsilon_1 - \epsilon_2 - \epsilon_3 = 0$. The square root in Eq. (4.6) must be real. This condition determines the limits x_{\pm} of the variable x . These limits can be written in the form

$$x_{\pm} = [b_3 \pm (b_3^2 - a_3 c_3)^{1/2}] a_3^{-1}, \quad (4.7)$$

where a_3 , b_3 , and c_3 are functions of ϵ_2 , ϵ_3 , and z , (cf. Jarp, Ref. 5). Since x_{\pm} must be real, we require $b_3^2 - a_3 c_3 \geq 0$, and this inequality gives

$$[\omega^2 - (\omega + m - \epsilon_2)^2 - |\vec{p}_2|^2 z^2] \epsilon_3^2 - 2(\omega + m - \epsilon_2)(\omega + m)(\epsilon_2 - m) \epsilon_3 + (\omega^2 + z^2 m^2) |\vec{p}_2|^2 - (\omega + m)^2 (\epsilon_2 - m)^2 - \omega^2 m^2 - 2z |\vec{p}_2| |\vec{p}_3| [(\omega + m - \epsilon_2) \epsilon_3 + (\omega + m)(\epsilon_2 - m) - \omega^2] \geq 0. \quad (4.8)$$

This condition determines the allowed values of ϵ_2 , ϵ_3 , and z . If we solve it with respect to ϵ_2 or ϵ_3 , we find fourth-order equations which are too complicated for complete analytical treatment. However, we may easily solve (4.8) with respect to z , and afterwards, determine the limits for ϵ_2 and ϵ_3 . Choosing a large number of combinations of allowed values for ϵ_2 and ϵ_3 , we could compute the corresponding limits of z , and thus find numerically, the minimum value of z for each photon energy ω . Allowed opening angles are determined by

$$z_- \leq z \leq 1, \quad (4.9)$$

and we show in Fig. 5 the dependence of z_- on ω . For comparison, we also show $x_- = 2(m/\omega)^{1/2}$, which gives the maximum angle between \vec{k} and the momentum of any of the final particles.

For a given, allowed value of z , the inequality (4.8) leads to a fourth-order equation for ϵ_3 , and the limits of ϵ_3 are determined by two of the roots of this equation. These roots depend on ϵ_2 , and by varying ϵ_2 and requiring that ϵ_3 be always in the region $m \leq \epsilon_3 \leq \omega - m - \epsilon_2$, we also obtain the

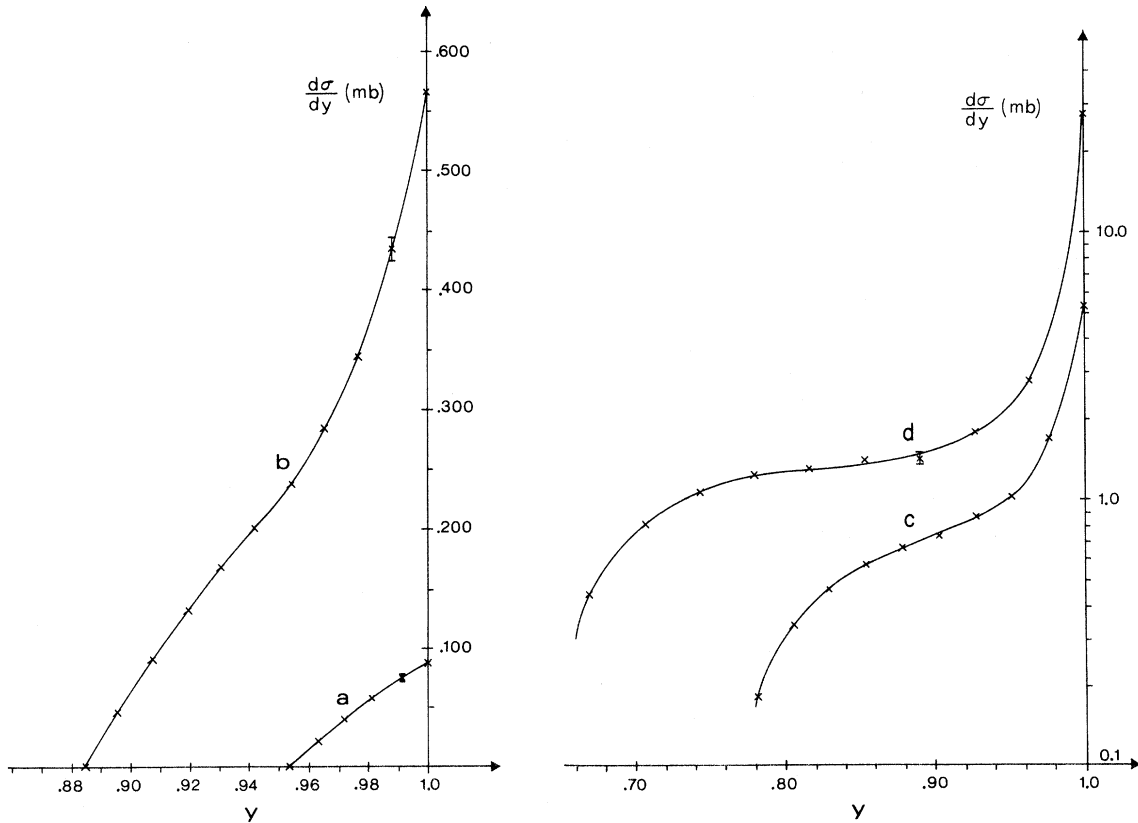


FIG. 4. The electron angular distribution $d\sigma/dy$, where $y = \cos \theta_-$, and θ_- is the angle between \vec{k} and \vec{p}_2 . The curves a, b, c, and d correspond to photon energies $\omega = 4.4, 5.12, 7.0$, and $10.0 mc^2$, respectively.

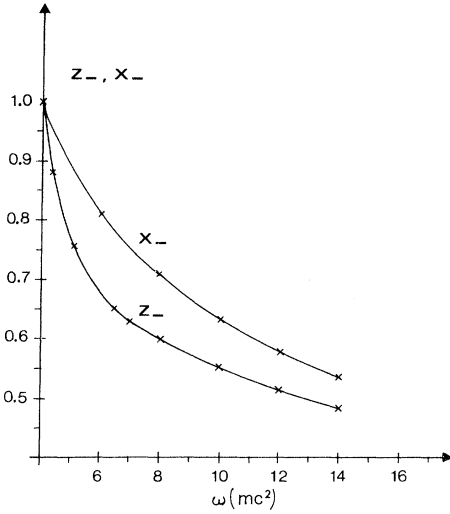


FIG. 5. The maximum opening angle $(\theta_{+-})_{\max}$ between positron and electron momenta, and the maximum angle θ_{\max} between photon momentum and the momentum of any of the final particles, as a function of photon energy ω in mc^2 . $z_- = \cos(\theta_{+-})_{\max}$, and $x_- = \cos\theta_{\max} = 2(m/\omega)^{1/2}$.

allowed values of ϵ_2 . Thus we are able to integrate the cross section, and resulting opening-angle distributions are shown in Fig. 6.

V. DOUBLE DIFFERENTIAL CROSS SECTIONS

We have prepared programs for calculating the cross sections $d^2\sigma/dxd\epsilon_3$, $d^2\sigma/dxd\epsilon_2$, $d^2\sigma/dyd\epsilon_2$, $d^2\sigma/dyd\epsilon_3$.

The cross section $d^2\sigma/dxd\epsilon_3$ which is differential in positron angle and energy, is easily obtained from Eq. (2.1) if we leave out the integration over x .

The cross section $d^2\sigma/dxd\epsilon_2$ which is differential in electron energy and positron angle, can be integrated if we use a method similar to the one described at the end of Sec. IV. This is necessary, since the kinematical relations again lead to complicated fourth-order equations for the limits of the variables.

The methods of integration for $d^2\sigma/dyd\epsilon_2$ and $d^2\sigma/dyd\epsilon_3$ are similar to the methods used for $d^2\sigma/dxd\epsilon_3$ and $d^2\sigma/dxd\epsilon_2$, respectively, since the phase space is symmetric in positron and electron variables.

In order to keep down the cost, we have only computed these double differential cross sections for one photon energy, $\omega = 5.12 mc^2$, which is the relevant energy for the Clermont experiment.⁴ The cross sections are shown in Figs. 7, 8, 9, and 10 as a function of the energies for electron

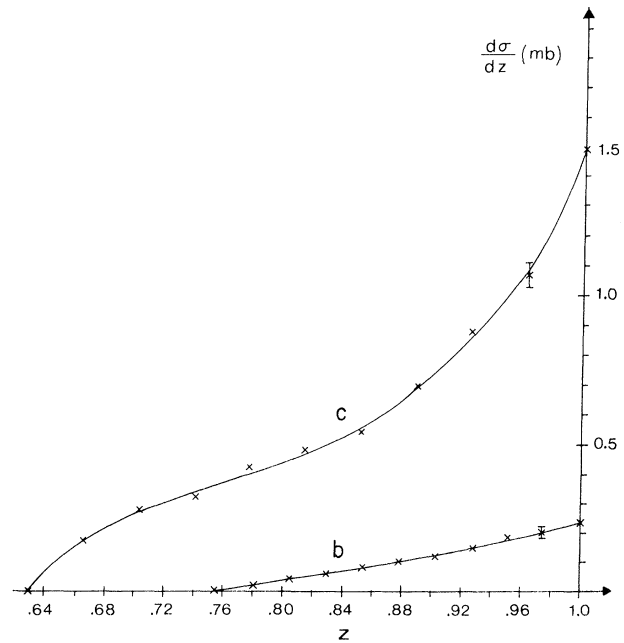
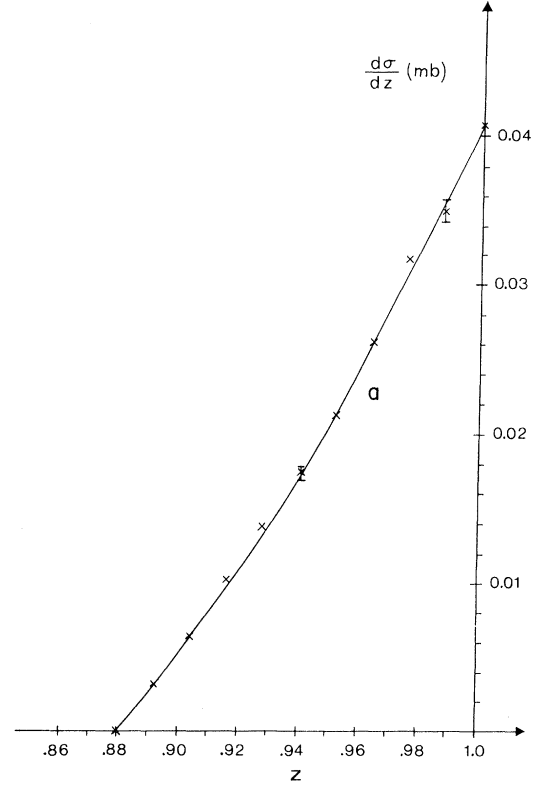


FIG. 6. The opening-angle distribution $d\sigma/dz$, where $z = \cos\theta_{+-}$ and θ_{+-} is the angle between the positron momentum and the momentum of one of the final electrons, as a function of z . The curves a, b, and c correspond to photon energies $\omega = 4.4, 5.12,$ and $7.0 mc^2$, respectively.

and positron angles given by $x = y = 1.0, 0.965, 0.930,$ and 0.895 .

Experimental values are not yet available for a comparison.

VI. CONCLUSION

The cross section for triplet production varies slowly with all variables for photon energies close to threshold, and it is easily integrated by simple numerical methods. As the photon energy increases, there is a strong peaking effect. The final particles are emitted close to the forward direction, and if this is not taken into account explicitly, large uncertainties appear in the numerical integrations. Our method of integration worked well for photon energies up to about $10 mc^2$, but for higher energies, the technique has to be refined.

The accuracy of our results is better than 5%. Characteristic rms errors obtained from the Monte Carlo method are shown on the figures. If the number of variables of integration was n , we

found that it was sufficient to compute the integrand about 10^n times in order to keep the errors below 5%.

From Fig. 1 we see that the positron energy distribution is almost symmetric about the mean energy. The electron spectra do not have this symmetry since here, lower energies are preferred, (cf. Fig. 2). It is interesting to compare the triplet energy spectra with the corresponding spectra obtained from pair production in a static Coulomb field. This is done in Fig. 11, where we show $d\sigma/d\epsilon_2$, $d\sigma/d\epsilon_3$, and $d\sigma_{\text{BH}}/d\epsilon_{\pm}$ for photon energy $\omega = 7.0 mc^2$. The last cross section is the symmetric Bethe-Heitler energy spectrum,⁶ and ϵ_{\pm} is the positron or the electron energy. We see that the triplet cross section is far below the Bethe-Heitler cross section, due to recoil and exchange effects. However, we have comparatively more low-energy electrons. This may be understood, since we have to produce in pair production, a low-energy electron together with a high-energy positron, while we already have in the triplet process, a low-energy electron in the initial state.

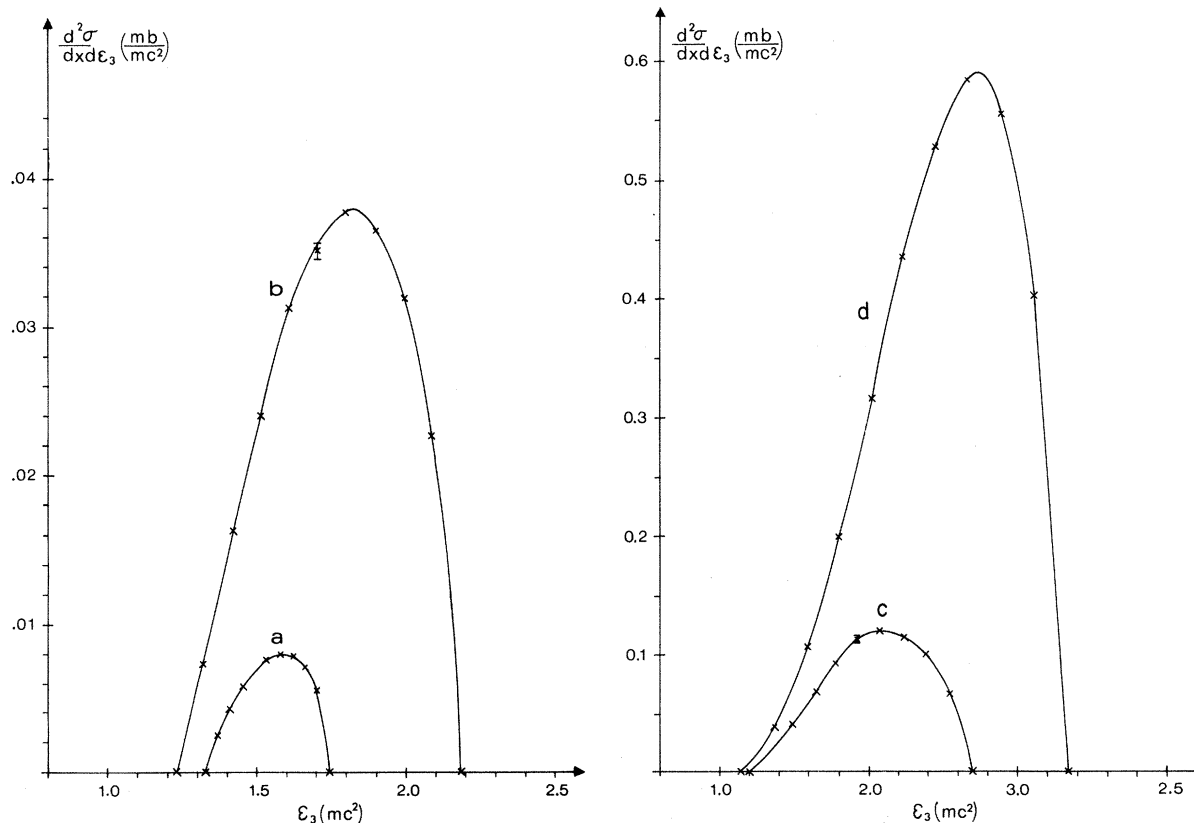


FIG. 7. The cross section $d^2\sigma/dx d\epsilon_3$, where ϵ_3 is the positron energy and $x = \cos\theta_+$, θ_+ is the angle between photon and positron momenta. Photon energy is $\omega = 5.12 mc^2$. The curves a, b, c, and d correspond to $x = 0.895, 0.930, 0.965,$ and 1.0 , respectively.

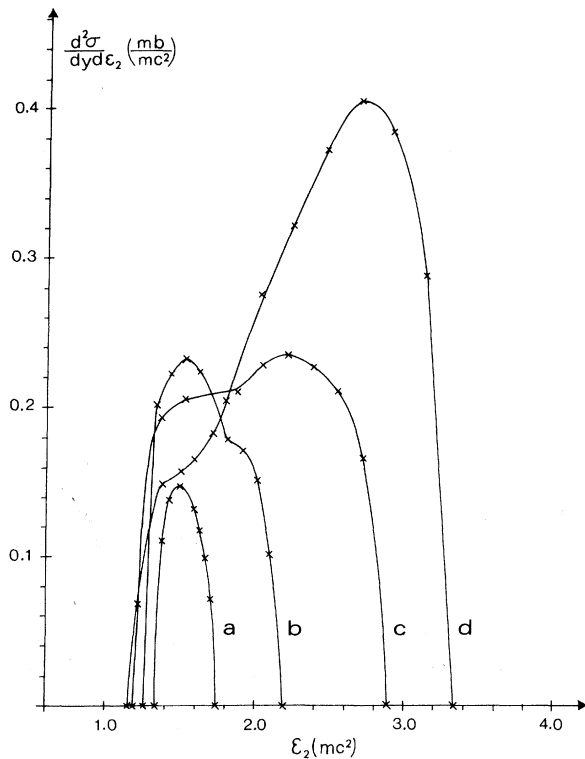


FIG. 8. The cross section $d^2\sigma/dy d\epsilon_2$, where ϵ_2 is the electron energy and $y = \cos\theta_-$, θ_- is the angle between photon and electron momenta. Photon energy is $\omega = 5.12 mc^2$. The curves a, b, c, and d correspond to $y = 0.895, 0.930, 0.977, \text{ and } 1.0$, respectively.

At the upper end of the triplet spectra, the positron and the electron distributions are equal. This is reasonable, since if one electron has high energy, the other electron must have low energy, and exchange effects are negligible. Therefore, we have symmetry between high-energy electrons and positrons.

The angular distributions given in Figs. 3 and 4 show that the importance of small angles increases with photon energy. The effect is more pronounced for positrons than for electrons. This is an effect of exchange, since the exclusion principle will cause the electrons to spread from each other, and therefore, also from the forward direction.

The results given in Figs. 7 and 8 show that we find more high-energy positrons and electrons as we approach the forward direction. This is a natural trend, since the total momentum is along this direction.

Figures 9 and 10 show the behavior of the cross sections which depend on one electron and one positron variable. The positron energy distribution is almost symmetrical about the mean energy independent of the electron direction. We see also

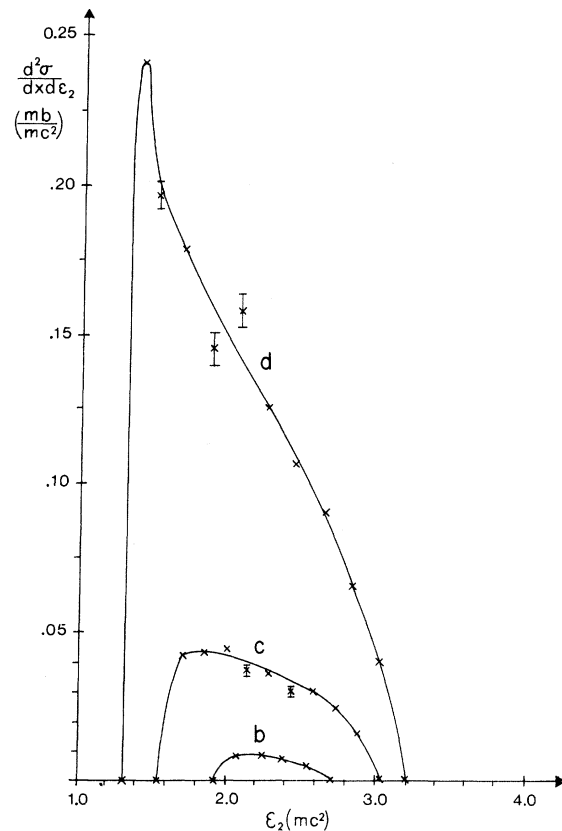
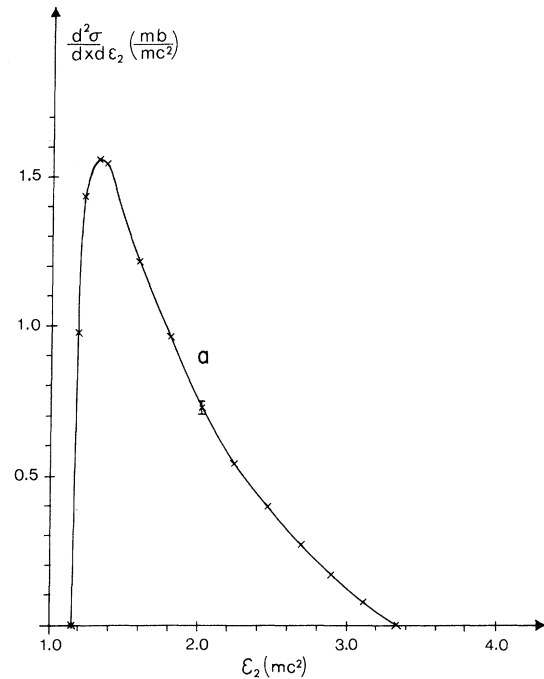


FIG. 9. The cross section $d^2\sigma/dx d\epsilon_2$. Photon energy is $\omega = 5.12 mc^2$. The curves a, b, c, and d correspond to $x = 0.895, 0.930, 0.965, \text{ and } 1.0$, respectively.

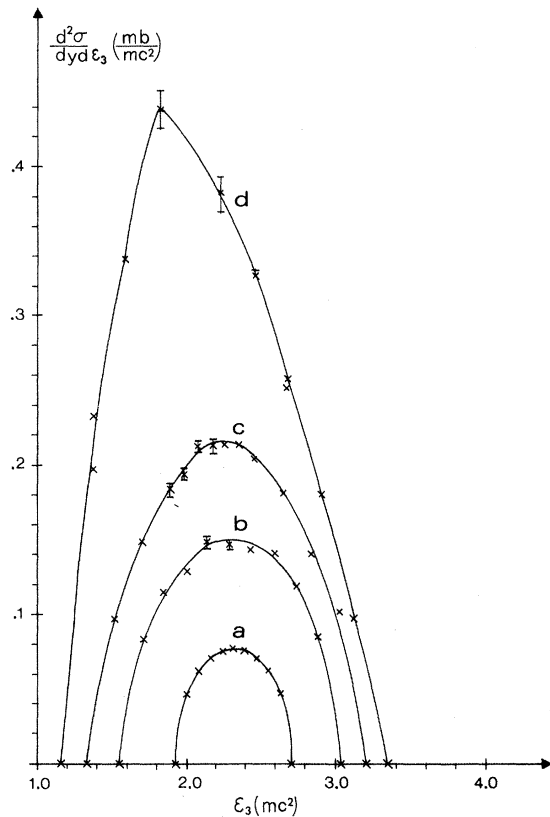


FIG. 10. The cross section $d^2\sigma/dy d\epsilon_3$. Photon energy is $\omega = 5.12 mc^2$. The curves a, b, c, and d correspond to $y = 0.895, 0.930, 0.965,$ and 1.0 , respectively.

that the average electron energy decreases strongly as the positron direction approaches the forward direction.

The results given above are valid for pair production on free electrons. Actual experiments are performed with electrons which are bound in atoms, and the theory should therefore, be corrected for effects of the nuclear field and the fields of other electrons in the atom. However, we expect that with the present accuracy of a few percent, these corrections can be neglected for low photon energies. The minimum energy of any of the final particles is given by Eq. (2.7). Calculating the corresponding minimum kinetic energy, we find this to be 13 keV and 78 keV, for photon energies $\omega = 10 mc^2$ and $5.12 mc^2$, respectively.

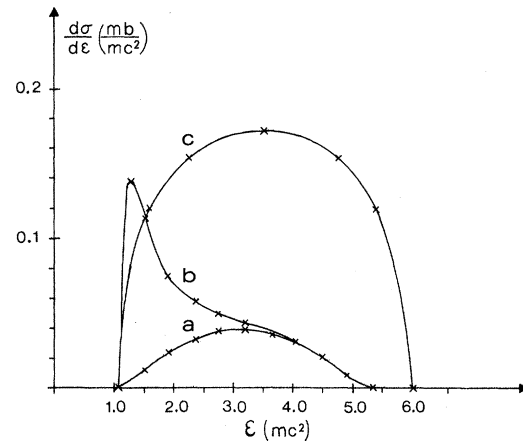


FIG. 11. The triplet positron and electron spectra $d\sigma/d\epsilon_3$ and $d\sigma/d\epsilon_2$ are given by curves a and b, respectively. The Bethe-Heitler energy spectrum for positrons or electrons, $d\alpha_{BH}/d\epsilon_{\pm}$, is given by curve c. Photon energy is $\omega = 7.0 mc^2$.

Thus, the energies of the final electrons are much larger than the binding energy of the initial electron, except for some electrons in very heavy atoms, and we therefore expect binding to be negligible.

Since the momentum transferred to the recoil electron is of order $1 mc$, the pairs are produced at impact parameters of order one Compton wavelength. Thus, the pairs are created close to the initial electron, where the field of this electron is dominating. Since the production occurs far from the nucleus and far from the other electrons in the atom, and since the final particles are fast, we expect Coulomb and screening corrections to be small.

Also radiative corrections are expected to be negligible. This is because radiative corrections are small at low energies in general, and also because triplet production is similar to pair production in the Coulomb field, and we know that for this process, the radiative corrections are of order 1%.⁷

ACKNOWLEDGMENTS

We are indebted to the streamer-chamber group at the University of Clermont for discussions concerning the triplet experiment.

*Present address: Defense Research Institute, Kjeller Norway.

¹K. J. Mork, Phys. Norv. 5, 51 (1971). In this paper the expression for the cross section contains an error.

The term $\kappa_0\sigma_1\sigma_2$ in V given by Eq. (1.10) should have a minus sign. This error also appears in formula 4B-3001 in the review article by J. W. Motz, H. A. Olsen, and H. W. Koch, Rev. Mod. Phys. 41, 581 (1969).

²K. J. Mork, Phys. Rev. 160, 1065 (1967).

³A. Borsellino, Nuovo Cimento 4, 112 (1947); Rev. Univ. Nac. Tucuman A 6, 7 (1947).

⁴G. Roche, J. Arnold, J. Augerat, L. Avan, M. Avan, J. Bonnet, J. Fargeix, A. Fleury, J. Jousset, M. L. Parizet, and M. Vialle, Nucl. Instrum. Methods (to be

published).

⁵Sverre Jarp, thesis, Trondheim, 1971 (unpublished).

⁶Ingjald Øverbø, thesis, Trondheim, 1970 (unpublished).

⁷K. Mork and H. Olsen, Phys. Rev. 140, B1661 (1965); 166, 1862 (1968).

PHYSICAL REVIEW D

VOLUME 8, NUMBER 1

1 JULY 1973

Dip in High-Energy pp Scattering and the Proton Substructure*

G. Eilam and Y. Gell

Department of Physics, McGill University, Montreal 101, Canada

(Received 17 January 1973)

The recently observed dip in high-energy elastic pp scattering is explained in the framework of models in which the nucleon possesses a layered substructure.

During recent years two types of models for high-energy elastic pp scattering have attracted much interest:

(a) geometrical and Regge versions of the diffractive model¹;

(b) models in which the proton exhibits a layered substructure.^{2,3}

An attractive feature of some of type (a) models is the dip, compatible with recent experimental results from the CERN Intersecting Storage Rings (ISR),⁴ which is predicted at high energy for $-2 \lesssim t \lesssim -1$ (GeV/c)².

It is quite interesting to see whether a similar dip pattern can be simply explained in the framework of type (b) models. The purpose of this paper is to show that a dip situated in the interval $-2.0 \lesssim t \lesssim -1.2$ (GeV/c)² is predicted from a type (b) model; it is also shown that the above result holds even including the single-flip amplitude.

It is well known that a finite sum of Gaussians provides an empirical fit to $d\sigma/dt$.² However, such a formula is theoretically unacceptable since it violates the Cerulus-Martin bound.⁵ This difficulty was overcome by Fleming, Giovannini, and Predazzi³ (hereafter FGP) who developed a theoretically consistent model and also obtained an excellent fit for $d\sigma/dt$ over the whole angular region at pre-ISR energies.

From the FGP approach, a picture emerged which visualizes the proton as possessing infinitely many layers. The higher the transverse momentum, the farther in the layer that gets excited in the collision.⁶

Furthermore, it was shown by FGP that at a given x , $x = \beta k \sin \theta \equiv \beta k_{\perp}$ (where β is the c.m. velocity of the proton, k is its c.m. momentum, and θ is the c.m. scattering angle), we expect an im-

portant contribution from the n th layer of the nucleon, where n increases like x^2 : $n \approx x^2/\Delta(x^2)$ [$\Delta(x^2)$ is the increment in x^2 for which a new region of interaction starts to be relevant]. Since a break in $d\sigma/dt$ which indicates a transition from the outermost layer to the second layer is observed at pre-ISR energies around $t \approx -1.2$ (GeV/c)²,⁷ one expects that for $-1.2 \lesssim t \lesssim 0$ (GeV/c)² only the outermost layer of the nucleon contributes significantly (note that $x^2 \approx -t$ at high energy and small angle). Thus, $\Delta(x^2) \approx 1.2$ (GeV/c)² and the second layer of the nucleon will give an important contribution for $-2.4 \lesssim t \lesssim -1.2$ (GeV/c)².

Let us now estimate the radii of the first two layers of the nucleon. Using Eq. (IV. 27) of FGP^{3,8} and taking 0.9 fm for the radius of the nucleon⁹ we find that the second layer of the nucleon is confined between $r_1 = 0.44$ fm and $r_2 = 0.33$ fm.¹⁰

In the following we show that, assuming the double-helicity-flip amplitudes to be negligible at high energies, the contribution of the second layer of the nucleon, which was found to be important for $-2.4 \lesssim t \lesssim -1.2$ (GeV/c)², is considerably reduced for all the other amplitudes for $-2.0 \lesssim t \lesssim -1.2$ (GeV/c)², and thus $d\sigma/dt$ is expected to exhibit a dip inside this t interval.

The partial-wave expansion for each one of the five independent helicity amplitudes $F_{\lambda_3 \lambda_4; \lambda_1 \lambda_2}$ (where λ_1, λ_2 and λ_3, λ_4 stand for the initial and final helicities, respectively) is given by

$$F_{\lambda_3 \lambda_4; \lambda_1 \lambda_2}(\cos \theta, s) = \frac{1}{k} \sum_0^{\infty} (2J+1) F_{\lambda_3 \lambda_4; \lambda_1 \lambda_2}^J(s) \times d_{\lambda \mu}^J(\cos \theta), \quad (1)$$

where $\lambda = \lambda_1 - \lambda_2$, $\mu = \lambda_3 - \lambda_4$. From the classical relation $J \approx kr$ (Ref. 11) and the previously stated